Emerging Applications of Interferometric Synthetic Aperture Radar (InSAR) in Geomorphology and Hydrology

Laurence C. Smith

Department of Geography, University of California, Los Angeles

Interferometric synthetic aperture radar (InSAR) is a powerful geodetic tool used to construct digital elevation models of the earth's topography and to image centimeter-scale displacements associated with crustal deformation and the flow of ice sheets. The past decade has seen significant improvements in our understanding of earthquakes, volcanoes, and glaciers as a direct result of this technology. Geomorphology and hydrology can also benefit from InSAR. A small but growing body of work shows that it is possible to interferometrically measure centimeter-scale motions associated with unstable slopes, land subsidence, fluctuating soil moisture and water levels, and deforming river-ice cover. Maps of interferometric correlation provide information about the structure of snow and reveal areas disturbed by erosion, sedimentation, flooding, snowfall, and aufeis growth. At present, such techniques are underdeveloped and largely overlooked by the geographic and radar communities. This article reviews these emerging geomorphic and hydrologic applications of InSAR and presents a first demonstration of motion detection for river ice. *Key Words: erosion, floods, hillslopes, interferometry, land subsidence, river ice, SAR, snow, soil moisture.*

The past decade has seen interferometric synthetic aperture radar (InSAR) progress from a pioneering technology to an accepted remote-sensing tool with diverse applications in the earth sciences. Early InSAR applications in the late 1980s and early 1990s included topography derivation (Graham 1974; Zebker and Goldstein 1986), and the measurement of ice-stream motion (Goldstein et al. 1993) and seismic strain (Massonnet et al. 1993; Zebker, Rosen, et al. 1994). Subsequent work in these areas has contributed to our understanding of earthquakes, vulcanism, ice-sheet dynamics, and land subsidence (see reviews by Gens and Van Genderen 1996; Madsen and Zebker 1998; Massonnet and Feigl 1998; Klees and Massonnet 1999; Bürgmann, Rosen, and Fielding 2000; Rosen et al. 2000; Zebker 2000).

The ability of InSAR to provide information that is useful to geomorphologists and hydrologists has been less recognized. A small but growing collection of studies suggests that slow slope motion, sediment erosion and deposition, soil and snow properties, water-level fluctuations, and river-ice motion can all be observed using InSAR. Some of these measurements are complementary to traditional field data. Others provide observations that are difficult to collect in the field, such as rates of soil creep over broad areas or maps of flood inundation made through clouds or during conditions of unfavorable meteorological conditions (notably wind). Much as InSAR mapping of crustal deformation (Massonnet et al. 1993; Zebker, Rosen, et al. 1994) and ice velocity (Goldstein et al. 1993) has impacted earthquake studies and glaciology, certain areas of geomorphology and hydrology are well positioned to benefit from this technology. For example, InSAR allows study of river systems in several different ways. Spatial patterns of flood erosion and sedimentation can be interferometrically mapped and, in some cases, their volumes can be determined (Smith et al. 2000). Simultaneous interferometric measurements of water-level fluctuations from hundreds of locations across an inundated, forested floodplain allow direct observation of how floodplains respond hydraulically to main-stem discharge (Alsdorf et al. 2000; Alsdorf, Smith, and Melack 2001). The subtle motions of winter river ice cover can also be interferometrically measured and related to ice mechanics and below-ice discharge conditions. These applications are in early stages of development.

This review aims to highlight these and other geomorphic and hydrologic uses of InSAR. To this end, the article begins with an introduction to InSAR fundamentals, including imaging geometry, data processing, and precision limits, and a comparison with photogrammetry, total station, global positioning systems (GPS), and airborne laser altimeter technologies. It then reviews seven emerging InSAR applications in geomorphology and hydrology: (1) slope motion; (2) land subsidence; (3) sediment erosion/deposition; (4) soil moisture; (5) river inundation; (6) snow cover, and (7) river ice, including

Annals of the Association of American Geographers, 92(3), 2002, pp. 385–398

Published by Blackwell Publishing, 350 Main Street, Malden, MA 02148, and 108 Cowley Road, Oxford, OX4 1JF, UK.

an original demonstration of the ability of InSAR to detect river-ice deformation. The discussion focuses on a collective assessment of these applications and identifies some promising areas for future research.

The Interferometric Method

This section provides an overview of InSAR imaging geometry, interferogram construction, and precision limits on derived digital elevation models (DEMs) and displacement maps. Because numerous reviews of the InSAR method and applications have now been published (Gens and Van Genderen 1996; Madsen and Zebker 1998; Massonnet and Feigl 1998; Klees and Massonnet 1999; Bürgmann et al. 2000; Rosen et al. 2000; Zebker 2000; Baltzer 2001), the section emphasizes aspects relevant to geomorphic and hydrologic studies.[1] In particular, interferometric correlation is described in some detail, owing to a growing use of this quantity in studies of surface change.

Interferograms, Displacement Maps, and Digital Elevation Models

Synthetic aperture radar (SAR) images are formed by recording the phase (time delay) and amplitude (energy intensity) of microwave echoes returned from the earth surface and assigning them locations in the image based on their return time and Doppler frequency shift. Traditional radar remote sensing utilizes only the amplitude portion of a single radar image (Figure 1A). In contrast,

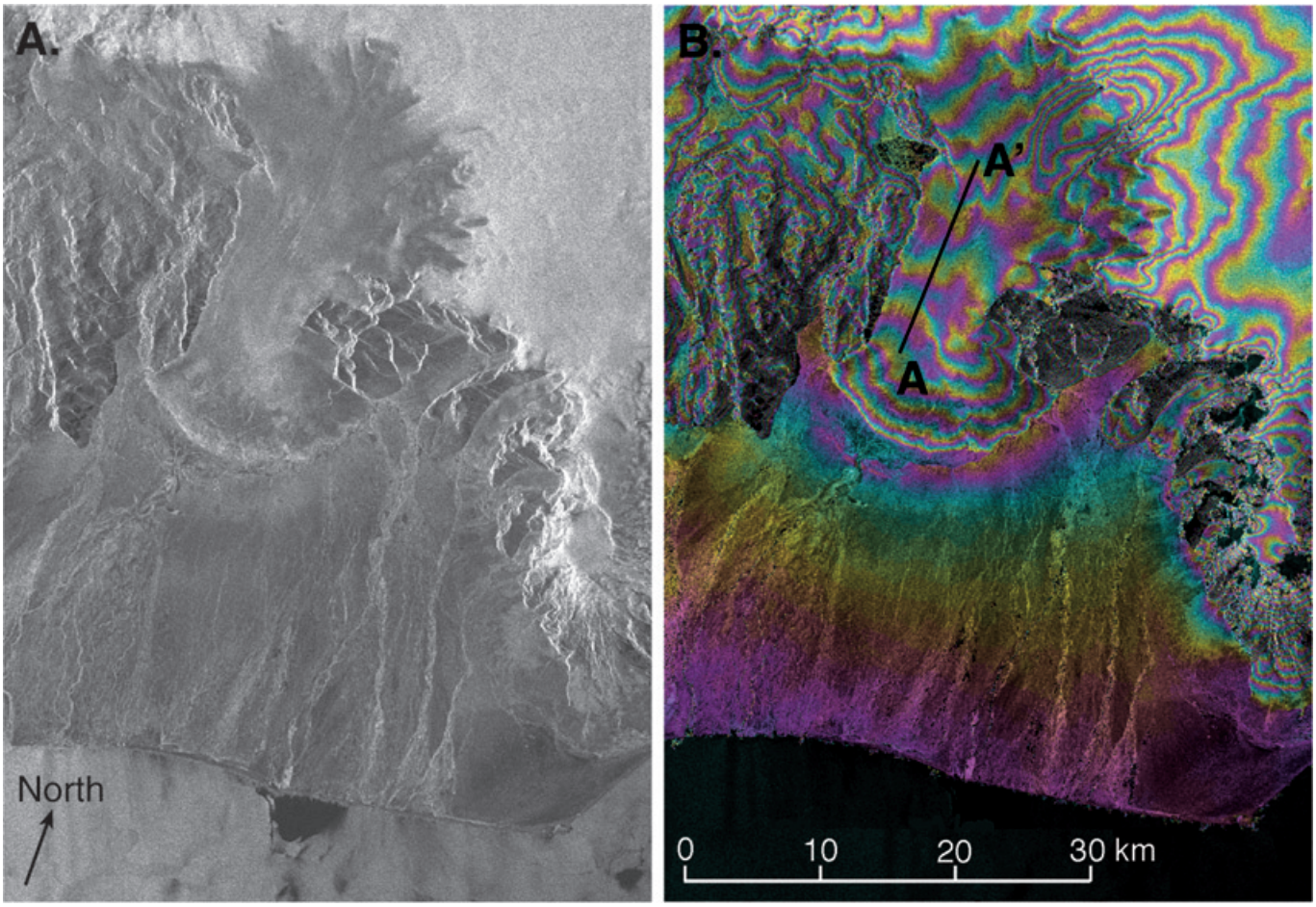

Figure 1. Synthetic aperture radar (A) amplitude image and (B) interferogram of the Skdeiðarárjökull glacier and its outwash plain, Iceland. Image centers are located at approximately 64N, 17W. Amplitude data were collected by a single ERS SAR overpass (1 January 1996) and show contrasts in surface roughness and moisture content. The interferogram is generated by subtracting the phase of a second image (2 January) from the phase of the 1 January image. Each color cycle represents a 0 to 2π cycle of interferometric phase. Patterns in the interferogram are largely caused by topographic relief. On the Skeiðarárjökull, additional cycles of interferometric phase are contributed by ice motion. Transect A-A' illustrates an example of phase unwrapping (described in the text section on "Interferograms, Displacement Maps, and Digital Elevation Models).

InSAR uses the phase values from two radar images. For a given point on the ground, the InSAR viewing geometry therefore consists of two SAR antenna positions separated by a short distance, or *baseline*, and the ground location. The phase measured by each SAR antenna is related to the number of wavelengths required to traverse the round-trip distance between the antenna and ground surface. Any ground motion that transpires in the radar line-of-sight direction between the times of the first and second images will introduce a small shortening or lengthening of round-trip distance, causing an offset in phase (see Zebker, Rosen, et al. 1994). This offset is readily seen by subtracting one phase image from another, yielding a map of interferometric phase called an *interferogram* (Figure 1B). Because the microwave signal must travel two ways, a line-of-sight displacement of one-half of a wavelength introduces one 2π cycle of interferometric phase to the interferogram. For example, SAR data from the ERS (European Remote Sensing) satellites is 5.66 cm in wavelength, so one cycle (0 to 2π) of interferometric phase is always equivalent to 2.33 cm of displacement in the line-of-sight direction, regardless of baseline. Centimeter-scale ground displacements are thus readily observed because they contribute directly to the phase shifts captured by an interferogram.

If the two SAR antenna positions are exactly the same (i.e., the baseline is zero), all interferometric phase may be attributed purely to ground displacements. However, as the baseline increases, additional cycles of interferometric phase are introduced to the interferogram due to parallax, even if ground motion has not occurred. The magnitude of this effect is controlled by baseline and surface relief. The topographic "equivalence" of one 2π cycle decreases nonlinearly with baseline (more specifically, the component of baseline that is perpendicular to the radar line of sight). Longer baselines increase this sensitivity to topography, generating even more cycles of interferometric phase in the interferogram for the same amount of relief. To illustrate how this effect controls the vertical precision of InSAR DEMs, consider the analogue of a topographic map. Much as the elevation interval represented by the contour interval of a topographic map decreases with increased map scale, the elevation interval represented by one 2π cycle of interferometric phase decreases with increased baseline. Therefore, short-baseline (zero to tens of meters) interferograms are optimal for detecting displacement because they are relatively insensitive to topography. Long-baseline (up to several hundred meters) interferograms are required for DEM construction; they are also sensitive to topography, as well as displacement.

Because interferometric phase values are only known between 0 and 2π (modulo 2π), adjacent 0 to 2π phase cycles must be cumulatively summed, or "unwrapped," across the interferogram to yield a new interferogram with values greater than 2π. This process is similar to "counting" contour lines on an unlabeled topographic map to obtain elevations. For example, the four interferometric phase cycles [$0\pi \rightarrow 2\pi$, $0\pi \rightarrow 2\pi$, $0\pi \rightarrow 2\pi$, $0\pi \rightarrow 2\pi$] along the transect A−A′ in Figure 1B may be unwrapped to values like [$6\pi \rightarrow 8\pi$, $8\pi \rightarrow 10\pi$, $10\pi \rightarrow 12\pi$, $12\pi \rightarrow 14\pi$]. If no motion has occurred, conversion of unwrapped interferometric phase to elevation is then a straightforward trigonometric computation based on the baseline orientation, antenna altitude, and SAR look angle. If motion has occurred, topographic and displacement contributions to the interferogram must be separated from each other before a DEM or displacement map can be made. This requires independent knowledge of static topography, from which the equivalent interferometric phase may be modeled and subtracted from the interferogram. In practice, this is achieved with an independent DEM or by subtracting a second "topography-only" interferogram (for which it is known that no motion has occurred), scaled by its baseline, from the first. Residual values of interferometric phase are then attributed to displacements in the radar line-of-sight direction. If the baseline is short, even a coarse-resolution DEM may be used, because a large interval of relief is required to generate a single cycle of interferometric phase.

It is important to recognize that limits to InSAR precision are millimeter-scale for measurements of *displacement*, but meter-scale for measurements of *elevation*. One reason for this difference is that displacements are determined solely from interferometric phase (which is measured to a fraction of a wavelength), whereas elevations are also controlled by baseline effects. Inexact knowledge of the baseline will therefore introduce errors to InSAR DEMs. Current satellite navigation and tracking technology does not allow the baseline to be determined exactly; instead, it is estimated using a variety of techniques (e.g., least-squares fitting of unwrapped phase to an existing DEM). Uncertainties in this estimate introduce systematic elevation errors to InSAR DEMs that typically range from meters to tens of meters. Furthermore, small errors in the estimate of the interferometric phase itself translate to large errors in derived elevation values. As example, this effect results in a minimum root-mean-square (rms) height error of 1.8 m for ERS DEMs (Zebker, Werner, et al. 1994). A third source of error results from temporal and spatial variations in atmospheric water-vapor content. Slight radar propagation delays can lead to significant height errors (tens to hundreds of meters) in InSAR DEMs and centimeter-

scale errors in displacement measurements (Goldstein 1995; Rosen et al. 1996; Zebker, Rosen, and Henley 1997). Such errors are spatially irregular, with length scales on the order of kilometers, corresponding to the scale of spatial variation in atmospheric water-vapor content. In practice, atmospheric effects are commonly mitigated by averaging multiple interferograms.

Interferometric Correlation

Because two or more radar images are required to calculate an interferogram, currently operating SAR satellites must return to image the same area twice. This method for constructing interferograms is often called "repeat-pass" interferometry.[2] The time lapse between image acquisitions is called the *temporal baseline*. Temporal baselines typically range from as short as one day (during the ERS "tandem" mission phases, in which one satellite follows the other) to as long as several years. Although there is no theoretical limit on the temporal baseline, it is commonly restricted to a few weeks or months due to some change in surface conditions that makes the radar images incoherent with each other. This phenomenon, called "decorrelation" or "coherence loss," precludes interferogram construction if sufficiently severe. As such, determination of interferometric correlation is a preliminary step in InSAR data processing and has previously been viewed as something of a data byproduct. More recently, interferometric correlation has proven useful for detecting a range of geomorphic and hydrologic processes that cause surface disturbance.

Two sets of co-registered radar echoes will be correlated with each other if each experiences the same or nearly the same interaction with scattering elements on the ground. This property is quantified by the total interferometric phase correlation c, calculated from two co-registered complex radar images i_1 and i_2 as:

$$c = \frac{\left|\langle i_1 i_2^* \rangle\right|}{\sqrt{\langle i_1 i_1^* \rangle \langle i_2 i_2^* \rangle}} \quad (1)$$

where asterisks denote complex conjugation and angular brackets denote statistical expectation, realized by spatial averaging within a user-defined filter. Correlation values for each pixel lie between 0 (no correlation) and 1 (perfect correlation). In practice, even uncorrelated surfaces display nonzero values of c due to the spatial averaging or "multilooking" of radar echoes required in InSAR processing. Provided that orbit trajectories are approximately parallel, instrument-noise levels stable and surface scattering dominant, loss of interferometric correlation between radar passes may be attributed to a temporal change in surface scattering properties (Zebker and Villasenor 1992). Examples include vegetation growth, erosion from water or wind, or a change in moisture conditions, each of which effectively presents a new set of scattering elements to the radar. Such processes change the scattering element geometry or dielectric properties, reducing interferometric correlation. Low correlation values ($c < \sim 0.3$) significantly reduce interferogram quality, precluding measurement of topography or motion. However, the correlation loss itself provides useful information about the temporal stability and/or scattering properties of the imaged surface. For this reason, interferometric correlation is experiencing increased use in vegetation, geomorphic, and hydrologic studies (Ichoku et al. 1998).[3]

Comparison with Laser, Photogrammetry, and GPS Methods

As described earlier, InSAR can measure deformation to within millimeters, but uncertainties in InSAR DEM elevations are on the order of meters. Imaging airborne laser altimeter systems can provide high-resolution DEMs with a vertical precision of around 10 cm, making them superior in quality to InSAR DEMs. However, to detect deformation, a second altimetric DEM must be obtained and subtracted from the first, resulting in rms errors that exceed 10 cm. Therefore, laser altimetry can produce more precise DEMs but less precise deformation maps than can InSAR. An additional consideration is that most airborne laser altimeters either are profiling instruments or obtain narrow swaths of data less than one kilometer in width. Therefore, numerous overlapping flight lines are required to construct a DEM comparable in area to those obtained using satellite InSAR.

Nearly all currently available U.S. Geological Survey 7.5 minute (30 m) DEMs are "Level-1" data derived from photogrammetric processing of aerial photographs acquired by the National High-Altitude Photography Program, the National Aerial Photography Program, or equivalent programs. Vertical and horizontal accuracy of these source data varies. However, to meet the Level 1 standard, an rms height error of 7 m is desired, with a maximum allowable value of 15 m. For absolute elevation, an error tolerance of 50 m is expected (U.S. Department of the Interior 1993). These specifications are met or exceeded by most InSAR DEMs, particularly in nonforested terrain. For the anticipated Shuttle Radar Topography Mission (SRTM) Level 2 Terrain Height Data Sets, absolute elevation accuracy will be better than 16 m. Estimates of even smaller, spatially varying errors will be provided in a separate image called a Random Height Error Data Set.

Ground-based surveys using GPS and laser total station technology can detect millimeter-scale deformation with precision comparable to or better than that provided by InSAR. In general, GPS provides superior estimates of horizontal displacement. Also, installation of permanent benchmarks allows slow deformation (e.g., tectonic motion) to be monitored for years without concern about surface decorrelation. The primary advantages of InSAR over GPS and total station methods are that measurements can be made in absence of fieldwork and that they are measured over broad areas, rather than point locations. However, it is important to keep in mind that displacements derived from a single interferogram are measured only in the radar line-of-sight direction. Decomposing this motion into vertical and horizontal components requires either additional interferograms with different viewing geometries or inference based on ground data.

Geomorphic Applications

The following section presents three geomorphic applications for InSAR displacement maps and DEMs. Topographic studies using a single InSAR DEM closely resemble traditional DEM analysis and are not discussed here. Instead, the section focuses on measurements of slow slope movement, land subsidence from fluid withdrawal or subterranean mining, and mapping and volumetric estimation of surface erosion and deposition.

Slow Slope Movement

Rapid landslides are difficult to measure interferometrically because they can deform the ground in excess of the phase gradient limit (Carnec, Massonnet, and King 1996) and commonly disturb the scattering surface, destroying interferometric correlation (Zebker et al. 1996; Massonnet and Feigl 1998). Also, SAR data are often of poor quality in areas of rugged relief due to radar foreshortening and layover effects. However, where slopes are moderate and interferometric correlation is preserved, slow slope movements can be measured using InSAR. Fruneau, Achache, and Delacourt (1996) generated six ERS-1 interferograms of a 1 km^2 landslide at the La Clapière landslide, near Saint-Étienne-de-Tinée in the southern French Alps. After each image pair is normalized to account for the time intervals between them, the interferograms are remarkably similar, suggesting steady-state downslope movements up to 30 mm day^{-1}. Spatial variations in the displacement field are also found, with a velocity decrease from top to bottom and significantly faster displacement on the western part of the landslide. A simple model of translational slide, accompanied by plastic deformation near structural discontinuities that cut the slide, satisfactorily explains the observed interferogram.

Carnec, Massonnet, and King (1996) report similar findings over the La Clapière landslide. However, they caution that they were unable to achieve similar success for another landslide nearby, and that the La Clapière site represents an optimal situation for detection of slope movement using InSAR. These conditions include a slow deformation rate that does not exceed the phase gradient limit and a near-grazing local incident angle. The latter produces an unusually fine ground-element resolution (approaching that of the slant-range resolution), allowing a small (less than 1 km^2) sliding slab to be effectively resolved.

Rott, Scheuchl, and Siegel (1999) detect much smaller displacements on a slowly creeping rock mass in the Öztal Alps, Austria. ERS interferograms spanning time periods of up to three years are used to detect downslope motion on the order of millimeters to centimeters per year. The interferometric observations are in good agreement with earlier ground-based geodetic measurements. Also revealed are previously undocumented creep on the upper slope and a three-fold interannual variation in motion, with fastest creep associated with a period of increased summer rainfall. Key to the study's success is the preservation of interferometric correlation over the one- to three-year time intervals required to detect such slow displacement, due in this case to the above-treeline location of the study site.

Ground Subsidence

InSAR studies of land subsidence in flat, arid terrain are more abundant and have generally achieved greater success than studies of slope movement in mountainous regions. It is now established that differential InSAR can image centimeter-scale ground subsidence caused by the removal of subsurface groundwater, petroleum, or coal. Most researchers have validated their interferometric observations with ground-based survey measurements with good success.

Van der Kooij (1997) used ERS repeat-pass image pairs with time separations ranging from 35 to 175 days to generate a composite map of subsidence caused by petroleum withdrawal at the Belridge and Lost Hills oil fields, about 100 km west of Bakersfield, California. Subsidence rates were steady between November 1995 and April 1996, yielding an extrapolated rate as high as 3000–4000 mm $year^{-1}$. Fielding, Blom, and Goldstein

(1998) also examine the area using ERS data, reporting similarly rapid rates of subsidence as high as 40 mm in 35 days, or >400 mm year^{-1}.

Also using ERS, Massonnet, Holzer, and Vadon (1997, 1998) find maximum subsidence of 18–19 mm year^{-1} at the East Mesa geothermal field, California, in good agreement with ground survey data. Integration of the InSAR-derived subsidence bowl yields a total volume of 4 million cubic meters, a value quite similar to an estimated 5 million cubic meters of net water withdrawal (including reinjection) between 1992 and 1994. At the Cerro Prieto geothermal field in Baja California, Mexico, Carnec and Fabriol (1999) find a maximum vertical deformation of 91 mm over 37 months (~280 mm year^{-1}) using interferograms from 1993 to 1997. Again, their InSAR observations are in good agreement with conventional leveling data. Furthermore, the observed fringe patterns are effectively reproduced by assuming elastic deformation in the subsurface with five spherical Mogi sources (Mogi 1958), confirming a theoretical model of subsurface withdrawal geometry.

Galloway and colleagues (1998) use ERS-1 data to image land subsidence in the Antelope Valley, located about 60 km northeast of Los Angeles in the Mojave Desert, California. Since 1926, aquifer compaction due to groundwater withdrawal has caused nearly 2 m of subsidence in the area. Despite the import of surface water and a reduction in agricultural consumption, water demand due to population growth and urbanization in the 1980s has led to groundwater withdrawals in excess of natural recharge, furthering land subsidence problems in the area. By assuming only the vertical component of displacement to be significant, they measured up to ~50 mm of subsidence between October 1993 and December 1995 (Figure 2). The InSAR-derived subsidence field corresponds well with the distribution and magnitude of subsidence simulated for the same period using a coupled model of groundwater flow and aquifer system compaction, and generally agrees with the historical pattern of subsidence measured between 1926 and 1992. An observed InSAR-derived subsidence of 40 mm compares well with the 42–49 mm computed for the site from a borehole extensometer that measures compaction in the 6–256 m depth interval below the land surface (Figure 2). The authors argue that in addition to detecting and quantifying land subsidence with a high degree of spatial and measurement resolution, InSAR can provide valuable insights into the distribution and magnitude of preconsolidation stress, vertical hydraulic conductivity, and the time constant for compacting aquifer systems, as well as their storage properties. These parameters are essential for the successful management and modeling of aquifer

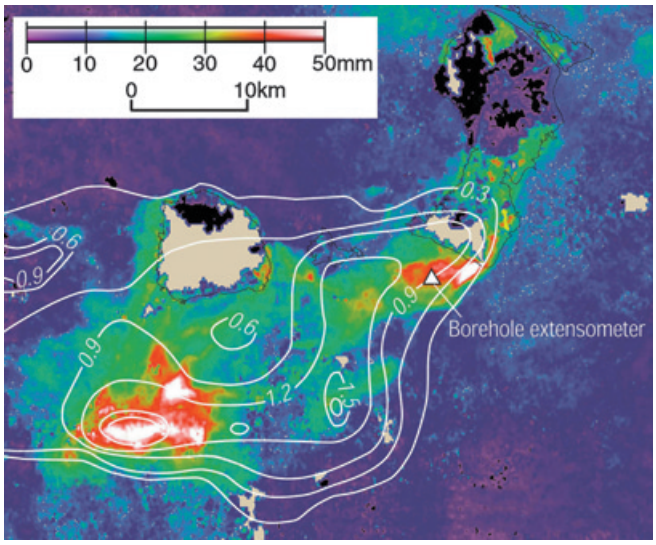

Figure 2. Interferometric (colored) and historical (contoured) observations of ground subsidence, Antelope Valley, California (35N, 118W). ERS InSAR measurements captured subsidence between 20 October 1993 and 22 December 1995. Historical observations (contours, in meters) span approximately 1930–1992. Beige colors signify temporal decorrelation; black colors signify regions of small-magnitude uplift. Adapted from Galloway and colleagues (1998).

compaction and resulting surface subsidence. Furthermore, it appears that InSAR can detect even small-magnitude, recoverable deformation that occurs at seasonal timescales, allowing estimation of elastic storage coefficients for aquifer systems (Hoffman et al. 2001).

Amelung and colleagues (1999) use a series of ERS interferograms to identify time-varying rates of subsidence caused by groundwater withdrawal in Las Vegas, Nevada. Periods of uplift associated with water-level recovery are also found. While spatial patterns of subsidence are similar in all interferograms, rates declined over the study period (from 70 mm between April 1992–November 1993 to 40 mm between November 1993–February 1996). The imaged deformation field further reveals that the spatial pattern of subsidence is controlled by Quaternary faults to a much greater degree than previously realized.

InSAR can also be used to detect the effects of subterranean mining on the overlying surface. Using a 35-day ERS interferogram, Carnec, Massonnet, and King (1996) measure up to 42 mm of subsidence over a coal field near Gardanne, France. This study was later extended to capture three years of subsidence from 1992 to 1995 in the area (Carnec and Delacourt 2000). By superimposing maps of underground mine workings on their interferograms, the authors observe migration of the surface subsidence halo caused by the advance of the coal-working

face. A similar methodology has been applied to the Selby coal field in the United Kingdom (Stow and Wright 1997). In a follow-up study, temporal averaging of ERS interferograms is used to track the extent and depth of a developing subsidence bowl, with depth increasing at about 400 mm/month (Wright and Stow 1999). Such methods are useful in environments that experience surficial change, because areas that experience decorrelation in one interferogram may be stable in another. They also reduce the need for phase-unwrapping (Sandwell and Price 1998) and allow detection of very slow, steady displacements that might otherwise be obscured by atmospheric effects or episodic events (e.g., Peltzer et al. 2001). However, in the case of land subsidence, additional difficulties are introduced where subsidence rates are large or features small (Raymond and Rudant 1997).

Erosion and Deposition

Two InSAR methods show promise for erosion and deposition studies. The first relies on the fact that interferometric correlation is destroyed by erosional or depositional processes that disturb the scattering surface, allowing the extent of disturbance to be mapped. The second employs subtraction of InSAR-derived DEMs to estimate volumes of net topographic change resulting from large erosional or depositional events.

While not expressly stated, the idea that temporal decorrelation can be used to detect surface erosion was probably first implied by Zebker and Villasenor (1992). Using L-band Seasat SAR data, they examine interferometric correlation for Death Valley over an eighteen-day period. Finding no decrease in correlation, they infer an absence of surface disturbance during the study period. Wegmüller and Werner (1995) interpret temporal decorrelation in a 14–29 September 1991 ERS image pair of the braided Tanana River, Alaska as "erosional tracks." In a more detailed study, Wegmüller and colleagues (2000) revisit Death Valley with ERS images acquired in 1993. Using a series of classification thresholds, they use variations in backscatter and correlation to define categories of stable and unstable surfaces, including erosion due to water or wind. They find an inverse linear relationship between field observations of unstable area fraction (i.e., the percentage area for which erosion is likely to occur) and interferometric correlation. By extrapolating this empirical relationship to other nonvegetated areas, they construct a map of erosional activity between 5 March and 14 May 1993. In an inverse approach, Smith and colleagues (2000) use *high* interferometric correlation to identify remnant floodplain fragments that survived sedimentary resurfacing by a 1996 catastrophic glacier outburst flood in Iceland.

Izenberg and colleagues (1996) use airborne TOPSAR data from the Jameson Island/Lisbon Bottoms, Missouri River to estimate net erosion caused by the record floods of 1993. Vertical errors in their airborne TOPSAR interferometric digital elevation model are estimated at 1–2 m, providing enough accuracy to compare preflood interferometric topography with postflood ground surveys. From height differences between the two, they estimate net scour of 4.7 million metric tons of sediment from levees and the river floodplain. In a similar approach relying solely on InSAR, Smith and colleagues (2000) present a methodology to estimate volumes of flood erosion or deposition, using ERS data from Skeiðarársandur, Iceland. The method requires ~4 m of topographic change to occur and should also be applicable to landslides. Centimeter-scale precision is not possible because sediment resurfacing destroys interferometric correlation in flooded areas, precluding construction of interferograms across the time of the flood. Instead, independent pre- and postevent InSAR DEMs are constructed, subjected to a correction procedure for height errors caused by baseline and atmospheric effects, and subtracted. This produces a three-dimensional map showing volumetric changes in surface topography resulting from an extreme flood (Figure 3). Integration of the map over defined areas yields estimates of $+38 \times 10^6$ m^3 of net sediment deposition along the ice margin, -25×10^6 m^3 of net erosion in channels downstream, and a total net balance of $+13 \times 10^6$ m^3 for the entire 40-km^2 study site.

Hydrologic Applications

The following section discusses applications of InSAR to studies of soil moisture, surface-water extent, snow cover, and river ice. Except for decorrelation mapping of surface water, all are in the early stages of development. InSAR applications in glaciology are well developed and have been reviewed elsewhere (Bindschadler 1998; Massonnet and Feigl 1998; Rosen et al. 2000; König, Winther, and Isaksson 2001). Along-track interferometry of ocean current velocity (which should also be applicable to inland rivers or large lakes) is also excluded from discussion, as this form of interferometry differs significantly from repeat-pass InSAR.[4]

Soil Moisture

Gabriel, Goldstein, and Zebker (1989) detect small phase shifts in Seasat data acquired over agricultural fields in

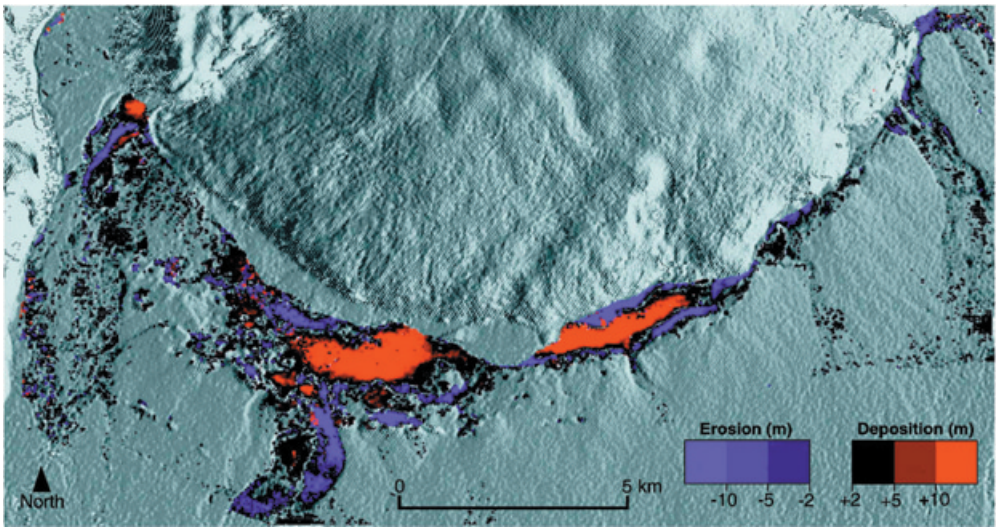

Figure 3. InSAR estimates of net erosion and deposition caused by an extreme glacier outburst flood in Iceland, 4–7 November 1996. Ice terminus is the Skeiðarárjökull glacier, also seen in Figure 1. Red hues indicate net deposition and blue hues signify net erosion. Pre- and post-flood ERS image pairs were acquired 21–22 October 1996 and 1–2 January 1997. From Smith et al. (2000).

the Imperial Valley, California. The observed centimeter-scale displacements conform closely with field boundaries and occur both toward and away from the radar. This effect is attributed to changing water content of hygroscopic clays—that is, the expansion of a field when watered or its contraction when dried. To test this hypothesis, the authors derive estimates of soil moisture content for 52 test sites derived from watering records of the Imperial Valley Water District. The ground data agree with the directions of interferometric displacement for 48 of the 52 sites. In subsequent studies with ERS, soil-swelling phenomena are noted for agricultural areas near Barstow, California (Zebker, Werner, et al. 1994), the Ukraine (Massonnet and Vadon 1995), the Netherlands (Gens and van Genderen 1996), the Imperial Valley again (Massonnet, Holzer, and Vadon 1997) and possibly in the Eureka Valley, California (Peltzer and Rosen 1995). However, despite the well-known sensitivity of InSAR to soil swelling, a focused study evaluating its potential for moisture retrievals or soil mapping has yet to be published.

Wegmüller (1997) uses ERS interferometric correlation over bare and sparsely vegetated agricultural fields in Middle Zeeland, The Netherlands, to aid remote estimation of soil moisture. Radar backscatter is sensitive to changing moisture content (from dielectric effects) and surface roughness. If surface roughness is fixed, all temporal changes in backscatter may be attributed to moisture effects. Because altering surface roughness (e.g., from plowing or vegetation growth) destroys interferometric correlation, presence of high correlation identifies where a backscatter-based moisture retrieval algorithm may be safely applied. Wegmüller employs this logic to successfully estimate soil moisture over fields with interferometric correlation greater than 0.7.

Inundation Extent and Water-Level Change

SAR appeals strongly to hydrologists as a tool for monitoring surface water due to its ability to obtain high-resolution imagery under all weather and illumination conditions. This characteristic is useful, for example, when observing floods during periods of monsoon cloud cover or shortening polar daylight. However, a primary limitation of SAR for detecting open water is caused by surface waves generated by wind or turbulence, particularly at C-band (Smith 1997). The resulting increase in surface roughness can raise backscatter amplitude values to levels similar to those from surrounding terrestrial areas, making lakes and rivers difficult or impossible to see in radar imagery. This problem is eliminated in interferometric correlation images. Because open water surfaces experience constant motion, C-band correlation is destroyed, allowing unambiguous mapping of open water bodies regardless of clouds, darkness, wind, or turbulence. This approach has been successfully used to obtain precise maps of river flooding in Siberia (Smith and Alsdorf 1997, 1998) and southern France (Marinelli et al. 1997), and to delineate wetland ecosystems on the Mackenzie River Delta (Hall-Atkinson and Smith 2001). In addition to low correlation, Strozzi and colleagues (2000) employ additional criteria of low backscatter

intensity and high temporal variability in backscatter intensity to classify water bodies in temporal SAR data.

In flooded forests and other floodplain environments in which rigid emergent vegetation is present, a double-bounce mechanism between trunks and water surface enhances radar backscattering to the satellite (Richards, Woodgate, and Skidmore 1987). This effect can maintain L-band correlation, allowing construction of interferograms over inundated areas. Observed interferometric phase values are then attributed to centimeter-scale changes in water level. Using L-HH SIR-C radar data collected by the space shuttle on 9–10 October 1994, Alsdorf and colleages (Alsdorf et al. 2000; Alsdorf, Smith, and Melack 2001) image subtle water level changes across ~3300 km^2 of the flooded Amazon River flood plain. Using InSAR observations from over 200 locations, they show that water levels in floodplain lakes and tributaries dropped 2–11 cm between orbits, with greatest drop magnitudes near the Amazon main-stem. A 12-cm drop was measured by the Amazon River gauging station at Manaus. Clearly, the interferometric observations capture the spatial pattern of floodplain water evacuation in response to a small drop in river stage. Alsdorf and colleagues (2001) further show that the method also works over large lakes, even with long time-separations between images. They combine radar altimeter and JERS-1 InSAR measurements to measure an average water level increase of 12 cm (corresponding to +280 m^3 of water storage) between 14 February and 30 March 1997 in Lake Balbina, a large man-made reservoir in the Amazon. It is particularly noteworthy that interferometric correlation was preserved over a 44-day time interval and that the presence of only 1–2 emergent tree trunks per SAR pixel (~25 m) was sufficient to produce the required double-bounce mechanism. Such evidence suggests that InSAR retrieval of water level change is a robust methodology.

Snow Cover Extent and Scattering Properties

Melt onset over snow surfaces is commonly associated with a sharp decrease in radar backscatter intensity. However, at low incident angles (e.g., ERS, at 23°), dry snow, wet snow with a rough surface, and snow with a thin wet surface layer can all yield similar backscatter intensities. Furthermore, soil freeze-thaw causes fluctuations in backscatter that can mimic wet snowfall. In recognition of the problems associated with backscatter-based snow mapping from single-parameter SAR such as ERS, Shi, Hensley, and Dozier (1997) examine interferometric correlation properties of snow cover at Mammoth Mountain, Sierra Nevada, California. Using SIR-C data acquired in April and October, they report strong correlation loss over April snow cover. This interpretation is validated with cloud-free Landsat thematic mapper data taken one day after the April SIR-C radar acquisition, with 86 percent agreement between Landsat and correlation-based snow cover classifications. Strozzi, Wegmüller, and Matzler (1999) use interferometric correlation to obtain unambiguous discrimination of wet snow cover for field and forest test sites in Middle Zeeland, The Netherlands and Bern, Switzerland. Time-series of interferometric correlation and backscatter intensity show that a wet snow cover dramatically reduces correlation, even when backscatter does not display a significant response. Furthermore, soil freeze-thaw is effectively separated from snowfall due to preservation of correlation in the former event, but not the latter.

Hoen and Zebker (2000) use ERS phase, backscatter, and interferometric correlation to estimate topography-induced variations in grain size and accumulation rate for a test site in the dry snow zone of the Greenland Ice Sheet. Because the total interferometric correlation c decreases with increased volume scattering, it is possible to infer snowpack scattering structure from correlation observations if the temporal and thermal contributions to c can be removed. Hoen and Zebker observe greater values of both correlation and backscatter intensity on the leeward sides of small-scale (~10 km) topographic undulations, suggesting reduced-volume scattering in the snowpack there. By employing simple modeling relating (1) snow grain size to backscatter and volume correlation and (2) the derived grain sizes to accumulation rate, they estimate variations in accumulation rate across the test site, finding a ~40 percent accumulation decrease in topographic lees.

River Ice

River-ice breakup and associated ice-jam flooding represent the most significant hydrological event of the year for most high-latitude rivers, with profound impacts upon biological activity, river loads of sediment and organic carbon, and water supply to perched lakes and other floodplain ecosystems. From a societal perspective, ice-jam floods are an unpredictable hazard that cause damages estimated at $100 million in the United States alone (White and Eames 1999). Pivotal to the study of river-ice breakup is the question of how and where mechanical ice breakup is initiated. We have now attained the capability to model and predict ice-debris accumulation and associated flooding levels caused by ice jams, given that the jam has formed somewhere (Pariset, Hauser, and Gagnon 1966; Uzuner and Kennedy 1976; Beltaos,

1984, 1993; Ferrick, Weyrick, and Nelson 1993; Ettema, Muste, and Kruger 1999). However, predicting *where* ice jams are likely to form is a question that remains intractable to date (Beltaos 1997). The problem is analogous to traffic flow: when a stop-and-start pattern of traffic flow is established, the location of where automobiles "pile up" is controlled by the location of where they previously "released." Similarly, successful prediction of ice jams location requires knowledge of where ice breakup will initiate. InSAR has already been used to detect small motions in sea ice (Dammert, Lepparanta, and Askne 1997, 1998; MacAyeal, Rignot, and Hulbe 1998; Rignot and MacAyeal 1998; Morris, Li, and Jeffries 1999). Similarly, it now appears likely that InSAR can detect centimeter-scale ice displacements prior to the breakup of river ice cover.

Shulyakovskii (1972) theorized that increased flow shear stress applied to the underside of the ice cover causes horizontal bending moments, owing to the meandering planform of most rivers. Bending stresses in excess of the flexural strength of the ice causes transverse fractures to occur, a process subsequently confirmed by field observations (Beltaos 1984, 1990). Vertical motions driven by increased river discharge typically occur along these fractures. Similarly, discharge decreases can cause collapse of the overlying ice cover. Figure 4 presents a first use of InSAR to detect both types of deformation on the frozen Ob' River, Siberia and the Mackenzie River Delta, Canada. Interferograms were generated from raw ERS signal data using the Gamma SAR Processor and Interferometry Software (Wegmüller and Werner 1997). SAR processing steps included range compression, autofocusing, and azimuth compression of raw ERS signal data. Interferometric processing included precise baseline estimation, image co-registration, estimation of interferometric correlation, 2×10 averaging in range and azimuth, interferogram computation, and phase-unwrapping. Motion detection was simplified by the fact that river ice is relatively flat, eliminating the need for an independent DEM or second interferogram to separate topographic and motion components. If "active" transverse fractures do indeed represent loci of subsequent ice breakup, Figure 4 demonstrates that InSAR may be used to identify where mechanical breakup is likely to initiate, providing a critical parameter needed to predict likely location of subsequent ice jam floods.

Aufeis mapping provides a second correlation-based application of InSAR to the study of river ice. Aufeis deposits—also called naleds, icings, or overflow ice—form annually on many rivers in high-latitude regions. These deposits may reach thicknesses of three meters or more in response to repeated episodes of overflow and freezing throughout the winter. Where large, they can significantly augment summer discharge due to their delayed melting period. Li and colleagues (1997) use a time series of tandem ERS correlation images to map aufeis growth for a test site in the Brooks Range, Alaska. As in the previously discussed snow-cover study by Strozzi and colleagues (1999), they find variable backscatter and low interferometric correlation over areas of aufeis formation. Correlation-derived estimates of aufeis area compare well with estimates from an earlier mapping study based on Landsat Multi-Spectral Scanner data (Dean 1984), but with better differentiation of spatial details such as channel structure.

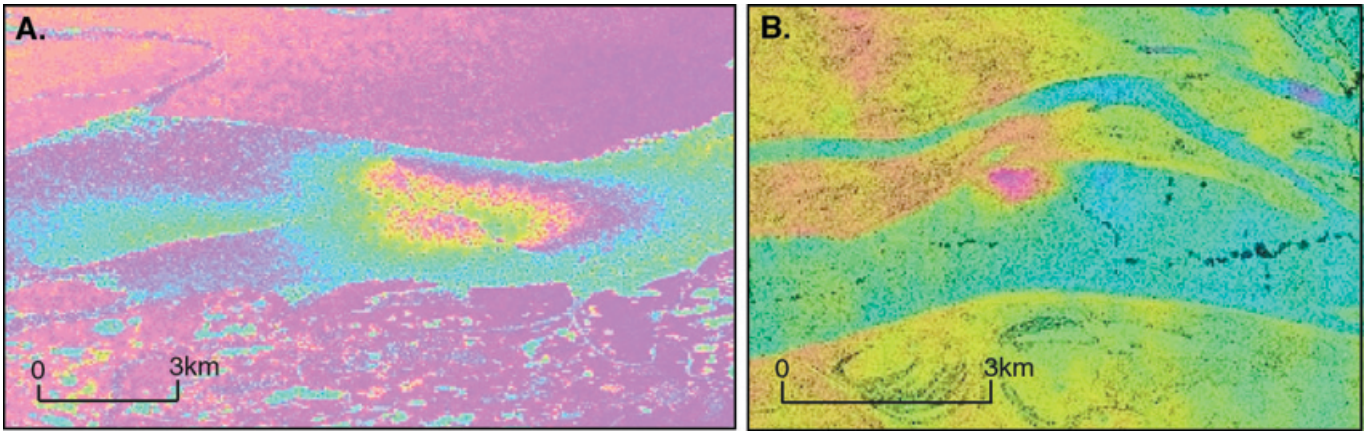

Figure 4. (A) ERS interferogram showing motion of river ice along transverse fractures, Mackenzie River Delta, Canada (68N, 135W). Line-of-sight displacements of 1–3 cm occurred between 22 and 23 January 1996. (B) Approximately 2 cm of localized ice collapse (reddish spot, center), Ob' River near Salekhard, Siberia (66N, 66E), again using tandem ERS data (26–27 March 1996). One color cycle of interferometric phase represents 2.3 cm of line-of-sight displacement for both interferograms.

Future Developments

InSAR is now being developed in novel ways to examine a variety of processes in geomorphology and hydrology. Of the emerging applications described here, land-surface subsidence caused by pumping or subterranean mining is best developed and should be widely applied in the near future for arid regions with low topographic relief. Urban centers are particularly well suited for long-term monitoring programs, as human dwellings maintain high interferometric correlation over time (Wegmüller and Werner 1995; Usai and Hanssen 1997; Carnec and Delacourt 2000; Strozzi et al. 2000). It also appears to be feasible to use InSAR for estimating the distribution and magnitude of a range of parameters needed to successfully model aquifer compression and associated surface subsidence, such as preconsolidation stress, compaction time constants, and elastic storage coefficients. InSAR studies of slope motion are more problematic, requiring a large mass waste with optimal orientation and incident angle, stable correlation properties through time, and a creeping rate of motion. However, if InSAR DEM subtraction can be used to measure extreme flood erosion (Figure 3), it may also be feasible to estimate landslide volumes if elevation changes exceed ~4 m and relief is moderate.

The ability of InSAR to observe centimeter-scale motions of shifting river ice, fluctuating water levels, and swelling soils has been demonstrated, but it requires further development. Mapping of water-level change (Alsdorf et al. 2000, 2001; Alsdorf, Smith, and Melack 2001) is particularly novel because it provides measurements from hundreds of locations in a single instant of time, unlike a river gauging station, which collects continuous data from a single location. Similarly, mapping of subtle river-ice deformation (Figure 4) is a new type of hydrologic observation that has not previously been demonstrated. Clearly, InSAR is more than a limited surrogate for certain field measurements, inasmuch as it also has the potential to provide fundamentally new types of observations. It is surprising that soil-swelling phenomena, first reported more than ten years ago (Gabriel, Goldstein, and Zebker 1989) and subsequently noted by many authors, have not been further exploited to estimate soil moisture or type: soil mapping applications would particularly benefit from the ability of InSAR to distinguish clay-rich hygroscopic soils from loams and sands that are less responsive to changing moisture.

Maps of interferometric correlation, once viewed as something of a byproduct of InSAR data-processing, hold promise for detecting a wide range of geomorphic and hydrologic processes that disturb the scattering surface, and the examples described here probably represent only a small fraction of possible applications. However, it is important to keep in mind that decorrelation, like displacement, is cumulative over time. Therefore, temporal baselines should be minimized to avoid occurrence of multiple (and therefore indistinguishable) disturbance events. Preservation of correlation over time can also be used to infer surface stability, such as undisturbed soils (Wegmüller 1997) or floodplain fragments that escape flood damage (Smith et al. 2000). "Stability studies" such as these represent a largely untapped area of research.

InSAR has achieved a high level of visibility in the geophysical sciences, thanks to a series of exciting discoveries in solid-earth and ice-sheet research. This has spurred InSAR research in other fields as well, including geomorphology and hydrology. The trend should continue as new applications emerge and InSAR becomes increasingly accessible to new users. Five years ago, InSAR processors (processing software) were limited in availability and often proprietary or prohibitively expensive. Today, there are a variety of freeware and commercial software packages from which to choose. However, even with improved software design and availability, generation of InSAR data products remains an often iterative and time-consuming process, and new users must anticipate an initial time investment to gain proficiency in InSAR data-processing. An excellent supply of suitable SAR data is available for the past ten years. The European Space Agency (ESA) has steadily archived suitable C-band SAR data with near-global coverage since the launch of the ERS-1 satellite in 1991. Archives of L-band JERS-1 SAR data are also maintained by the National Space Development Agency of Japan (NASDA). However, ERS-2 has recently experienced yaw pointing uncertainties of ± 10 degrees, making the resulting SAR data unsuitable for interferometry. It is unclear whether this problem will be resolved in the future, and in any event ERS-2 has now exceeded its design lifetime. The currently operating Canadian RADARSAT provides useable SAR data, but lack of zero doppler steering (which keeps the radar beam perpendicular to the flight path) makes interferometry a chance affair. However, the current reduction in InSAR data collection should be resolved by planned satellite missions that include Envisat (launched by the ESA in March 2002) and ALOS (scheduled for launch by NASDA in 2003). Both will be capable of interferometry and should assure a continued supply of suitable InSAR data as we enter the twenty-first century.

Acknowledgments

This work was supported by the NASA New Investigator Program (grant NAG5-10609). Figure 2 was adapted

from a figure provided by D. Galloway, U.S. Geological Survey. The author thanks D. Alsdorf, B. Bauer, M. Bulmer and one anonymous reader for their constructive reviews of this article.

Notes

1. For additional background, see rigorous treatments of topography derivation (Graham 1974; Zebker and Goldstein 1986; Madsen, Zebker, and Martin 1993; Zebker, Werner, et al. 1994), displacement mapping (Gabriel, Goldstein, and Zebker 1989; Zebker, Rosen, et al. 1994; Joughin, Kwok, and Fahnestock 1998), and phase-unwrapping (Goldstein, Zebker, and Werner 1988; Zebker and Lu 1998).
2. Note that interferograms can be recovered immediately from a single platform if two radar antennae are used, such as those deployed by the February 2000 Shuttle Radar Topography Mission.
3. For further description of interferometric correlation and its properties, see Zebker and Villasenor (1992), Rignot and Van Zyl (1993), and Rosen et al. (2000).
4. Gens and Van Genderen (1996) and Rosen et al. (2000) give brief descriptions of this application.

References

Alsdorf, D. E., C. Birkett, T. Dunne, J. Melack, and L. Hess. 2001. Water-level changes in a large Amazon lake measured with spaceborne radar interferometry and altimetry. *Geophysical Research Letters* 28 (14): 2671–74.

Alsdorf, D. E., J. M. Melack, T. Dunne, L. A. K. Mertes, L. L. Hess, and L. C. Smith. 2000. Interferometric measurements of water level changes on the Amazon flood plain. *Nature* 404:174–77.

Alsdorf, D. E., L. C. Smith, and J. M. Melack. 2001. Amazon water-level changes measured with interferometric SIR-C radar. *IEEE Transactions on Geoscience and Remote Sensing* 39 (2): 423–31.

Amelung, F., D. L. Galloway, J. W. Bell, H. Zebker, and R. J. Laczniak. 1999. Sensing the ups and downs of Las Vegas: InSAR reveals structural control of land subsidence and aquifer-system deformation. *Geology* 27 (6): 483–86.

Balzter, H. 2001. Forest mapping and monitoring with interferometric synthetic aperture radar (InSAR). *Progress in Physical Geography* 25 (2): 159–77.

Beltaos, S. 1984. A conceptual model of river ice breakup. *Canadian Journal of Civil Engineering* 11 (3): 516–29.

———. 1990. Fracture and breakup of river ice cover. *Canadian Journal of Civil Engineering* 17 (2): 173–83.

———. 1993. Numerical computation of river ice jams. *Canadian Journal of Civil Engineering* 20 (1): 88–99.

———. 1997. Onset of river ice breakup. *Cold Regions Science and Technology* 25:183–96.

Bindschadler, R. 1998. Monitoring ice-sheet behavior from space. *Reviews of Geophysics* 36:79–104.

Bürgmann, R., P. A. Rosen, and E. J. Fielding. 2000. Synthetic aperture radar interferometry to measure Earth's surface topography and its deformation. *Annual Review Earth Planetary Sciences* 28:169–209.

Carnec, C., and C. Delacourt. 2000. Three years of mining subsidence monitored by SAR interferometry, near Gardanne, France. *Journal of Applied Geophysics* 43:43–54.

Carnec, C., and H. Fabriol. 1999. Monitoring and modeling land subsidence at the Cerro Prieto geothermal field, Baja California, Mexico, using SAR interferometry. *Geophysical Research Letters* 26 (9): 1211–14.

Carnec, C., D. Massonnet, and C. King. 1996. Two examples of the use of SAR interferometry on displacement fields of small extent. *Geophysical Research Letters* 23 (24): 3579–82.

Dammert, P. B. G., M. Lepparanta, and J. Askne. 1997. Sea-ice displacements measured by ERS-1 SAR interferometry. *European Space Agency Special Publication ESA SP–414, Proc. 3rd ERS Symposium, 17–21 March 1997, Florence, Italy*, comp. T.-D. Guyenne and D. Danesy, 923–930. Noordwijk, The Netherlands: ESA Publications Division, ESTEC.

Dammert, P. B. G., M. Lepparanta, and J. Askne. 1998. SAR interferometry over Baltic Sea ice. *International Journal of Remote Sensing* 19 (16): 3019–37.

Dean, K. G. 1984. Stream-icing zones in Alaska. *Report on Investigations, State of Alaska, Department of Natural Resources, Division of Geological and Geophysics Surveys* 84 (16): 1–20.

Ettema, R., M. Muste, and A. Kruger. 1999. *Ice jams in river confluences*. CRREL Report 99–6. Hanover, NH: U.S. Army Corps of Engineers, Cold Regions Research and Engineering Laboratory.

Ferrick, M. G., P. B. Weyrick, and D. F. Nelson. 1993. Kinematic model of river-ice motion during dynamic breakup. *Nordic Hydrology* 24:111–34.

Fielding, E. J., R. G. Blom, and R. M. Goldstein. 1998. Rapid subsidence over oil fields measured by SAR interferometry. *Geophysical Research Letters* 25 (17): 3215–18.

Fruneau, B., J. Achache, and C. Delacourt. 1996. Observation and modelling of the Saint-Etienne-de-Tinée landslide using SAR interferometry. *Tectonophysics* 265:181–90.

Gabriel, A. K., R. M. Goldstein, and H. A. Zebker. 1989. Mapping small elevation changes over large areas: Differential radar interferometry. *Journal of Geophysical Research* 94 (B7): 9183–91.

Galloway, D. L., K. W. Hudnut, S. E. Ingebritsen, S. P. Phillips, G. Peltzer, F. Rogez, and P. A. Rosen. 1998. Detection of aquifer system compaction and land subsidence using interferometric synthetic aperture radar, Antelope Valley, Mojave Desert, California. *Water Resources Research* 34 (10): 2573–85.

Gens, R., and J. L. Van Genderen. 1996. SAR interferometry—Issues, techniques, applications. *International Journal Remote Sensing* 17 (10): 1803–35.

Goldstein, R. M. 1995. Atmospheric limitations to repeat-track interferometry. *Geophysical Research Letters* 22 (18): 2517–20.

Goldstein, R. M., H. Engelhardt, B. Kamb, and R. M. Frolich. 1993. Satellite radar interferometry for monitoring ice sheet motion: Application to an Antarctic ice stream. *Science* 262:1525–30.

Goldstein, R. M., H. A. Zebker, and C. L. Werner. 1988. Satellite radar interferometry: Two dimensional phase unwrapping. *Radio Science* 23:713–20.

Graham, L. C. 1974. Synthetic interferometer radar for topographic mapping. *Proceedings of the IEEE* 62:763–68.

Hall-Atkinson, C., and L. C. Smith. 2001. Delineation of delta ecozones using interferometric SAR phase coherence,

Mackenzie River Delta, N.W.T., Canada. *Remote Sensing of Environment* 78:229–38.

Hoen, E. W., and H. A. Zebker. 2000. Topography-driven variations in backscatter strength and depth observed over the Greenland Ice Sheet with InSAR. *Proceedings IEEE Geoscience and Remote Sensing Symposium (IGARSS '00)* 2:470–72.

Hoffman, J., H. A. Zebker, D. L. Galloway, and F. Amelung. 2001. Seasonal subsidence and rebound in Las Vegas Valley, Nevada observed by synthetic aperture radar interferometry. *Water Resources Research* 37 (6): 1551–66.

Ichoku, C., A. Karnieli, Y. Arkin, J. Chorowicz, T. Fleury, and J.-P. Rudant. 1998. Exploring the utility potential of SAR interferometric coherence images. *International Journal of Remote Sensing* 19 (6): 1147–60.

Izenberg, N. R., R. E. Arvidson, R. A. Brackett, S. S. Saatchi, G. R. Osburn, and J. Dohrenwend. 1996. Erosional and depositional patterns associated with the 1993 Missouri River floods inferred from SIR-C and TOPSAR radar data. *Journal of Geophysical Research* 101 (E10): 23149–67.

Joughin, I. R., R. Kwok, and M. A. Fahnestock. 1998. Interferometric estimation of three-dimensional ice flow using ascending and descending passes. *IEEE Transactions on Geoscience and Remote Sensing* 36 (1): 25–37.

Klees, R., and D. Massonnet. 1999. Deformation measurements using SAR interferometry: potential and limitations. *Geologie en Mjinbouw* 77:161–76, 196–201.

König, M., J.-G. Winther, and E. Isaksson. 2001. Measuring snow and glacier ice properties from satellite. *Reviews of Geophysics* 39 (1): 1–27.

Li, S., C. Benson, L. Shapiro, and K. Dean. 1997. Aufeis in the Ivishak River, Alaska, mapped from satellite radar interferometry. *Remote Sensing of Environment* 60:131–39.

MacAyeal, D. R., E. Rignot, and C. L. Hulbe. 1998. Ice-shelf dynamics near the front of the Filchner-Ronne Ice Shelf, Antarctica, revealed by SAR interferometry: model/interferogram comparison. *Journal of Glaciology* 44 (147): 419–28.

Madsen, S. N., and H. A. Zebker. 1998. Imaging radar interferometry. In *Principles and applications of imaging radar*, vol. 2, *Manual of remote sensing*, ed. F. M. Henderson and A. J. Lewis, 359–79. 3rd ed. New York: John Wiley & Sons.

Madsen, S. N., H. A. Zebker, and J. Martin. 1993. Topographic mapping using radar interferometry: Processing techniques. *IEEE Transactions on Geoscience and Remote Sensing* 31:246–56.

Marinelli, L., R. Michel, A. Beaudoin, and J. Astier. 1997. Flood mapping using ERS tandem coherence image: A case study in southern France. *European Space Agency Special Publication ESA SP-414, Proc. 3rd ERS Symposium, 17–21 March 1997, Florence, Italy*, 531–36.

Massonnet, D., and K. L. Feigl. 1998. Radar interferometry and its application to changes in the Earth's surface. *Reviews of Geophysics* 36 (4): 441–500.

Massonnet, D., T. Holzer, and H. Vadon. 1997. Land subsidence caused by the East Mesa geothermal field, California, observed using SAR interferometry. *Geophysical Research Letters* 24 (8): 901–4.

Massonnet, D., T. Holzer, and H. Vadon. 1998. Correction to "Land subsidence caused by the East Mesa geothermal field, California, observed using SAR interferometry." *Geophysical Research Letters* 25 (16): 3213.

Massonnet, D., M. Rossi, C. Carmona, F. Adragna, G. Peltzer, K. Feigl, and T. Rabaute. 1993. The displacement field of the Landers earthquake mapped by radar interferometry. *Nature* 364:138–42.

Massonnet, D., and H. Vadon. 1995. ERS-1 internal clock drift measured by interferometry. *IEEE Transactions on Geoscience and Remote Sensing* 33 (2): 401–8.

Mogi, K. 1958. Relations between eruptions of various volcanoes and the deformation of the ground surface around them. *Bulletin Earthquake Research, Inst. Univ. Tokyo* 36:99–134.

Morris, K., S. Li, and M. Jeffries. 1999. Meso- and microscale sea-ice motion in the East Siberian Sea as determined from ERS-1 SAR data. *Journal of Glaciology* 45 (150): 370–83.

Pariset, E., R. Hauser, and A. Gagnon. 1966. Formation of ice covers and ice jams in rivers. *ASCE Journal of Hydraulic Engineering* 92 (HY6): 1–24.

Peltzer, G., F. Crampe, S. Hensley, and P. Rosen. 2001. Transient strain accumulation and fault interaction in the Eastern California Shear Zone. *Geology* 29 (11): 975–78.

Peltzer, G., and P. Rosen. 1995. Surface displacement of the 17 May 1993 Eureka Valley, California earthquake observed by SAR interferometry. *Science* 268:1333–36.

Raymond, D., and J.-P. Rudant. 1997. ERS1-SAR interferometry: Potential and limits for mining subsidence detection. *European Space Agency Special Publication ESA SP-414, Proc. 3rd ERS Symposium, 17–21 March 1997, Florence, Italy*, 541–44.

Richards, J. A., P. W. Woodgate, and A. K. Skidmore. 1987. An explanation of enhanced radar backscattering from flooded forests. *International Journal of Remote Sensing* 8 (7): 1093–100.

Rignot, E. J. M., and D. R. MacAyeal. 1998. Ice-shelf dynamics near the front of the Filchner-Ronne Ice Shelf, Antarctica, revealed by SAR interferometry. *Journal of Glaciology* 44 (147): 405–18.

Rignot, E. J. M., and J. J. van Zyl. 1993. Change detection techniques for ERS-1 SAR data. *IEEE Transactions on Geoscience and Remote Sensing* 31 (4): 896–906.

Rosen, P. A., S. Hensley, I. R. Joughin, F. K. Li, S. N. Madsen, E. Rodríguez, and R. Goldstein. 2000. Synthetic aperture radar interferometry. *Proceedings of the IEEE* 88 (3): 333–82.

Rosen, P. A., S. Hensley, H. A. Zebker, F. H. Webb, and E. J. Fielding. 1996. Surface deformation and coherence measurements of Kilauea Volcano, Hawaii, from SIR-C radar interferometry. *Journal of Geophysical Research* 101 (E10): 23109–25.

Rott, H., B. Scheuchl, and A. Siegel. 1999. Monitoring very slow slope movements by means of SAR interferometry: A case study from a mass waste above a reservoir in the Ötztal Alps, Austria. *Geophysical Research Letters* 26 (11): 1629–32.

Sandwell, D. T., and E. J. Price. 1998. Phase gradient approach to stacking interferograms. *Journal of Geophysical Research* 103 (B12): 30183–204.

Shi, J., S. Hensley, and J. Dozier. 1997. Mapping snow cover with repeat-pass synthetic aperture radar. *Proceedings IEEE Geoscience and Remote Sensing Symposium (IGARSS '97)* 2:628–30.

Shulyakovskii, L. G., 1972. On a model of the break-up process. *Soviet Hydrology Selected Papers* 1:21–27.

Smith, L. C. 1997. Satellite remote sensing of river inundation area, stage, and discharge: A review. *Hydrological Processes* 11:1427–39.

Smith, L. C., and D. E. Alsdorf. 1997. Flood mapping from phase decorrelation of ERS tandem data: The Ob' River, Siberia.

European Space Agency Special Publication ESA SP–414, Proc. 3rd ERS Symposium, 17–21 March 1997, Florence, Italy, 537–39.

Smith, L. C., and D. E. Alsdorf. 1998. A control on sediment and organic carbon delivery to the Arctic Ocean revealed with satellite SAR: Ob'River, Siberia. *Geology* 26 (5): 395–98.

Smith, L. C., D. E. Alsdorf, F. J. Magilligan, B. Gomez, L. A. K. Mertes, N. D. Smith, and J. B. Garvin. 2000. Estimation of erosion, deposition, and net volumetric change caused by the 1996 Skeiðarársandur Jökulhlaup, Iceland, from SAR interferometry. *Water Resources Research* 36 (6): 1583–94.

Stow, R. J., and P. Wright. 1997. Mining subsidence land survey by SAR interferometry. *European Space Agency Special Publication ESA SP–414, Proc. 3rd ERS Symposium, 17–21 March 1997, Florence, Italy*, 525–30.

Strozzi, T., U. Wegmüller, and C. Matzler. 1999. Mapping wet snow covers with SAR interferometry. *International Journal of Remote Sensing* 20 (12): 2395–403.

Strozzi, T., P. B. G. Dammert, U. Wegmüller, J.-M. Martinez, J. I. H. Askne, A. Beaudoin, and M. T. Hallikainen. 2000. Land-use mapping with ERS SAR interferometry. *IEEE Transactions on Geoscience and Remote Sensing* 38 (2): 766–75.

U. S. Department of the Interior. 1993. U.S. Geological Survey. *Data user's guide 5—Digital elevation models*. Reston, VA: U.S. Department of the Interior.

Usai, S., and R. Hanssen. 1997. Long time-scale INSAR by means of high coherence features. *European Space Agency Special Publication ESA SP–414, Proc. 3rd ERS Symposium, 17–21 March 1997, Florence, Italy*, 225–28.

Uzuner, M. S., and J. F. Kennedy. 1976. Theoretical model of river ice jams. *ASCE Journal of Hydraulic Engineering* 102 (HY9): 1364–83.

Van der Kooij, M. 1997. Land subsidence measurements at the Belridge oil fields from ERS InSAR data. *European Space Agency Special Publication ESA SP–414, Proc. 3rd ERS Symposium, 17–21 March 1997, Florence, Italy*, 1853–58.

Wegmüller, U. 1997. Soil moisture monitoring with ERS SAR interferometry. *European Space Agency Special Publication ESA SP–414, Proc. 3rd ERS Symposium, 17–21 March 1997, Florence, Italy*, 47–52.

Wegmüller, U., T. Strozzi, T. Farr, and C. L. Werner. 2000. Arid land-surface characterization with repeat-pass SAR interferometry. *IEEE Transactions on Geoscience and Remote Sensing* 38 (2): 776–81.

Wegmüller, U., and C. L. Werner. 1995. SAR interferometric signatures of forest. *IEEE Transactions on Geoscience and Remote Sensing* 33 (5): 1153–61.

Wegmüller, U., and C. L. Werner. 1997. Gamma SAR processor and interferometry software. *European Space Agency Special Publication ESA SP–414, Proc. 3rd ERS Symposium, 17–21 March 1997, Florence, Italy*, 1687–92.

White, K. D., and H. J. Eames. 1999. *CRREL ice jam database*. CRREL Report 99–2. Hanover, NH: U.S. Army Corps of Engineers, Cold Regions Research and Engineering Laboratory.

Wright, P., and R. Stow. 1999. Detecting mining subsidence from space. *International Journal of Remote Sensing* 20 (6): 1183–88.

Zebker, H. 2000. Studying the Earth with interferometric radar. *Computing in Science and Engineering* 2 (3): 52–60.

Zebker, H., and R. Goldstein. 1986. Topographic mapping from interferometric synthetic aperture radar observations. *Journal of Geophysical Research* 91 (B5): 4993–99.

Zebker, H., and Y. P. Lu. 1998. Phase-unwrapping algorithms for radar interferometry: Residue-cut, least-squares, and synthesis algorithms. *Journal of the Optical Society of America-A* 15 (3): 586–98.

Zebker, H., P. A. Rosen, R. M. Goldstein, A. Gabriel, and C. L. Werner. 1994. On the derivation of coseismic displacement fields using differential radar interferometry: The Landers earthquake. *Journal of Geophysical Research* 99 (B10): 19617–34.

Zebker, H., P. Rosen, S. Hensley, and P. J. Mouginis-Mark. 1996. Analysis of active lava flows on Kilauea volcano, Hawaii, using SIR-C radar correlation measurements. *Geology* 24 (6): 495–98.

Zebker, H., P. Rosen, and S. Hensley. 1997. Atmospheric effect in interferometric synthetic aperture radar surface deformation and topographic maps. *Journal of Geophysical Research* 102 (B4): 7547–63.

Zebker, H., and J. Villasenor. 1992. Decorrelation in interferometric radar echoes. *IEEE Transactions on Geoscience and Remote Sensing* 30 (5): 950–59.

Zebker, H., C. L. Werner, P. A. Rosen, and S. Hensley. 1994. Accuracy of topographic maps derived from ERS-1 interferometric radar. *IEEE Transactions on Geoscience and Remote Sensing* 32 (4): 823–36.

Correspondence: Department of Geography, University of California, Los Angeles, Los Angeles, CA 90095-1524, e-mail: lsmith@geog.ucla.edu.